Indonesian Journal of Aerospace Vol. 22 No. 2 Desember 2024 : pp 103 – 118 (Salaswati et al.)
DOI: 10.59981/ijoa.2024.3090
https://ejournal.brin.go.id/ijoa/

A Review of Absolute Radiometry Calibration Method for Satellite Multispectral Camera while in Orbit

Sartika Salaswati[1,2], Adhi Harmoko Saputro[1], Wahyudi Hasbi[2]

[1]Department of Physics, Faculty of Mathematics and Natural Sciences, Universitas Indonesia, Indonesia
[2]Research Center for Satellite Technology, National Research and Innovation Agency (BRIN), Indonesia
e-mail: sartika.salaswati21@ui.ac.id / sartika.salaswati@brin.go.id

Received: 04-01-2024. Accepted: 23-09-2024. Published: 20-05-2025

Abstract

Multispectral cameras on satellites are a type of camera that is widely used in satellite remote sensing and has wide applications. Therefore, it is necessary to carry out absolute radiometric calibration to maintain the accuracy of radiometric information in satellite camera images. There are several types of absolute radiometric calibration, including onboard, Rayleigh, vicarious, and cross-calibration. These methods have strengths and weaknesses. Therefore, it is necessary to conduct a literature review to find out which calibration method is appropriate for certain conditions. Based on a literature review, all methods can be used and adapted to the conditions of the satellite. The onboard calibration method is suitable for satellites equipped with calibration instruments. The Rayleigh calibration method is suitable for large FOV cameras with visual wavelengths. The vicarious calibration method is suitable for satellites from countries close to standardized calibration sites. Meanwhile, the cross-calibration method is suitable for satellites cameras that have specifications and conditions close to the reference camera. Therefore, these calibration methods can be carried out together to complement each method.

Keywords**:** *onboard, Rayleigh, vicarious, cross, calibration*

1. Introduction

A multispectral camera is a camera that works with the spectral imaging method in several spectral channels. In the imaging process, a multispectral camera has wavelengths that do not overlap and consists of more than three spectral channels. Spectral imaging offers several advantages, namely fast, accurate, low cost, and simple operation. Apart from that, this system is also flexible and suitable for analyzing the composition of a sample (Ariza Ramirez et al., 2022). Multispectral cameras have higher spatial resolution and less distortion than hyperspectral cameras (Hao et al., 2023). Recently, the use of multispectral cameras has become a suitable method for analyzing and controlling food quality. In addition, it's also popular in the aerospace and military industries (Mishra et al., 2022). In aerospace, multispectral cameras are widely used in satellite remote sensing.

Multispectral cameras are a type of camera that is widely used in satellite remote sensing. This camera is used for remote sensing satellites, such as LANDSAT (Ridwan et al., 2018), Sentinel, and Terra/Aqua satellites. Multispectral cameras in satellite remote sensing are used for detection and characterization of agroforestry systems (Bolívar-Santamaría & Reu, 2021), assessment of land-use change (Parveen & Ilahi, 2022), identify ground vegetation (Fadaei, 2020), mangrove forest mapping (Sharifi et al., 2022) (Thakur et al., 2020) (Tamang et al., 2022), assessment of forest restoration (C. C. Liu et al., 2019), and evaluation for the sustainable development of an urban area (Prasad et al., 2022).

Because of the utilization, camera images must have good quality in geometry and radiometry. Radiometrically, an image is considered high quality if the radiance of an object in the camera image has the same value as the actual radiance (the result of direct measurement of the object on Earth). Geometrically, an image is considered high quality if an object in the image is in its actual position on Earth. Therefore, calibration is carried

out to maintain this quality on satellite cameras.

Based on the launch time, radiometric calibration is divided into pre-launch and post-launch calibration. Meanwhile, based on its output, radiometric calibration is divided into relative and absolute calibrations. Relative calibration is the visual calibration of the image, while in absolute radiometry calibration, the most important thing is to convert digital numbers (DN) of satellite images into reflectance or radiance on Top of the Atmosphere (TOA) (Han, Tao, Xie, Li, et al., 2021). In this research, absolute radiometric calibration is the research focus because this type of calibration plays a direct role in the utilization of remote sensing satellite imagery. The use of remote sensing satellite imagery requires input in the radiometric units such as reflectance or radiance, which are the final outputs of absolute radiometric calibration.

There are several methods of absolute radiometry calibration, such as onboard calibration, Rayleigh calibration, vicarious calibration, and cross-calibration. The calibration methods have strengths and weaknesses. Onboard calibration produces more precise calibration coefficients, but the calibration system will degrade over time (Xu et al., 2020). Rayleigh calibration is suitable for wide Field of View (FOV) cameras, but it is only for visual channels (Zhu et al., 2019). Vicarious calibration is precise, but it requires expensive costs and measurement operators (Y. Liu et al., 2018). Cross-calibration can be done frequently, but it is difficult to equalize conditions between cameras. Therefore, it is necessary to conduct a literature review to find out which calibration method is appropriate for the condition of the satellite camera to be calibrated.

2. Radiometry Calibration

Radiometry calibration is a calibration technique to avoid radiometric distortion. When electromagnetic waves are emitted or reflected on an optical sensor, the electromagnetic energy is distorted by both the optical sensor and the atmosphere. Radiometry calibration consists of absolute and relative radiometric calibration. Relative calibration is calibration that focuses on the process of improving the image visually. In relative calibration, a vignetting correction process is performed on the image so that the image has the same response in each pixel. The vignetting effect is a darker effect that occurs at the corners of the image compared to the center of the image. According to references, the difference in response between pixels after relative calibration is <1% (Ryan & Pagnutti, 2009).

After relative calibration is performed, absolute calibration is then carried out. Absolute calibration is calibration that connects the digital number (DN) of the image with radiance. This calibration is crucial for remote sensing satellites because the radiation measured by the camera will be separated from the influence of the atmosphere (Ryan & Pagnutti, 2009). The purpose of this calibration is to obtain calibration constants. It can be used to convert the digital number (DN) of images into reflectance or radiance values for an area (Thome, 2001). This calibration is carried out before launch (laboratory) and after launch (in-orbit).

Laboratory calibration is conducted using a uniform light source with a known radiance value. In this calibration, the measurement camera's response to variations in light is carried out. Light variation can be obtained from the variation of the light source itself or from camera parameters such as gain and exposure time. Additionally, measurements are taken of the camera in dark conditions (un-illuminated) to determine the real Digital Number (DN) value of the camera. Spectral measurements are also conducted for each camera channel to ensure the spectral characteristics of the camera. Once these processes are completed, the calibration coefficient can be determined. This calibration coefficient is the result of laboratory calibration and can be used to convert DN values into radiance. The laboratory calibration process is illustrated in Figures 2-1 and 2-2.

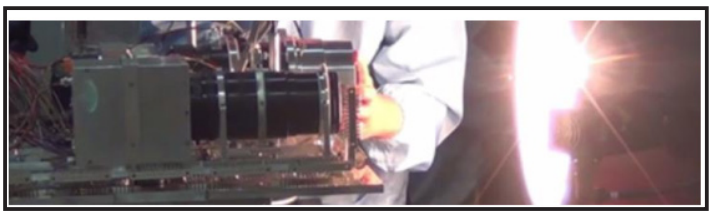

Figure 2-1. Camera Responsivity Measurement

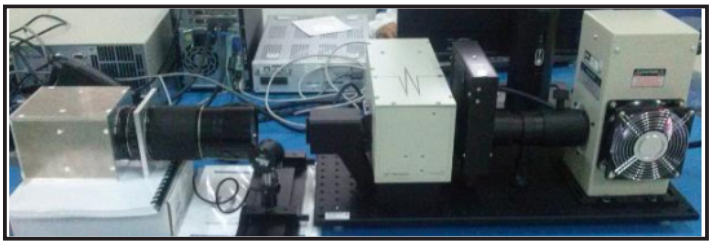

Figure 2-2. Camera Spectral Measurement

Conceptually, in-orbit absolute radiometric calibration has the same goal as absolute radiometric calibration in the laboratory. However, the difference lies in the light source used. In laboratory radiometric calibration, the light source is directly in front of the camera and its value is precisely known. In contrast, for some in-orbit radiometric calibrations, the light source is sunlight illuminating the calibration site and received by the camera, necessitating atmospheric correction to determine the actual radiance value. To achieve a uniform radiance value similar to laboratory calibration, a uniform and standardized calibration site is required.

A region can be considered a calibration site if it meets the following requirements: the area is generally homogeneous, does not change over time, and has low rainfall (Teillet, P.; Chander, 2010). Additionally, the area should be free of cloud cover, have low aerosol levels, and be located at a high elevation to minimize atmospheric influence. Typically, these areas have little human activity. This region or site is ensured to remain a calibration/validation area through quality control (Hu et al., 2020). Some standardized calibration sites are listed in Table 2-1, and an example of a calibration site can be seen in Figure 2-3.

Table 2-1. Calibration Sites PICS and RadCalNet (Bacour et al., 2019) (Alhammoud et al., 2019)

	Sites	Latitude (°)		Longitude (°)		Characteristic
		Max	Min	Max	Min	
PICS	Algeria-3	30.50	30.20	7.60	7.30	There are sand dunes with a height of 100 meters. The spatial variability is <3% over 100 kilometers
	Algeria-5	31.20	30.90	2.50	2.20	
	Libya-1	24.80	24.50	13.60	13.30	
	Libya-4	28.65	28.42	23.02	22.80	
	Mauritania-1	19.60	19.40	-9.20	-9.40	The lowest spatial variability compared to other PICS regions
	Mauritania-2	20.60	20.40	-8.50	-8.80	
Rad-Cal-Net	Baotou, Cina	40.85	40.84	109.63	109.62	Spatial variability is <3% and temporal variability is <2% over an area of <20 km.
	Gobabeb, Namibia	-23.59	-23.60	15.12	15.11	
	La Crau, Prancis	43.56	43.55	4.86	4.86	
	Railroad Valley Playa, USA	38.50	38.49	-115.68	-115.69	

Figure 2-3. Gobabeb Calibration Site, Namibia (Sinclair et al., 2020)

In-orbit calibration needs to be performed periodically because there is a possibility of changes in the camera sensor over time. Several methods need to be employed to complement the shortcomings of each calibration method, resulting in accurate calibration coefficients with efficient methods. One of the absolute radiometric calibration methods in orbit can be seen in Figure 2-4.

Figure 2-4. Measurement of Reflectance and Atmospheric Properties in Vicarious Calibration

3. Absolute Radiometry Calibration in Orbit

This paper focuses more on in-orbit radiometric calibration to facilitate the comparison process between different types of the same radiometric calibration. There are several methods on absolute radiometry calibration for satellite multispectral cameras while in orbit, including the on-board calibration method, Rayleigh distribution calibration, vicarious calibration, and cross-calibration.

3.1. On-board Calibration

Basically, cameras on remote sensing satellites are calibrated before launch. However, there is a possibility that changes will occur due to vibrations during launch, space radiation, or temperature while in orbit. A calibration system is needed to guarantee the quality of the camera. The calibration system is claimed to have high accuracy is on-board calibration. On-board calibration is calibration using a calibration device installed on the satellite. This method has advantages in terms of lighting and observation conditions. This method also has the advantage of high calibration frequency and accuracy (Song et al., 2022).

Advanced Spaceborne Thermal Emission and Reflection (ASTER), one of the payloads of the Terra satellite, uses a light-based calibrator to monitor change in sensor response. ASTER calibration uses two halogen lamps periodically. The lamp and optical system calibration are monitored by a silicon photo monitor. In addition, before the satellite launched, the on-board calibration system was characterized by an integrating sphere and black body (Arai, 2013a).

In addition to monitoring changes in sensor response, the on-board radiometric calibration system also carries out spectral calibration and degradation observations, such as in the HY-1C Satellite Calibration Spectrometer (SCS) calibration system. This satellite calibration system uses on-board spectral calibration based on a wavelength diffuser. Like the ASTER calibration system, the HY-1C carries out measurements at the diffuser wavelength with a standard spectrum (Xu et al., 2020).

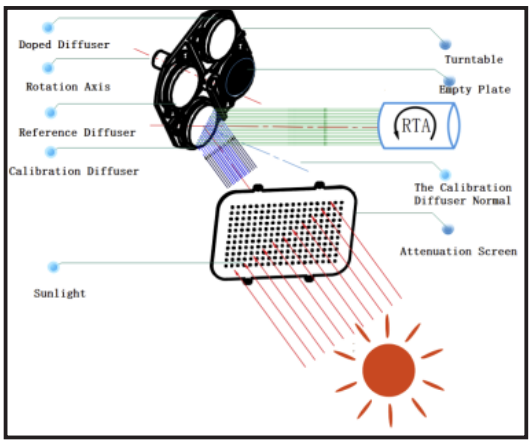

Figure 3-1. On-board Calibration System on SCS satellite HY-1C

The SCS on-board calibration system consists of a calibration wheel and solar attenuation screen to reduce solar energy entering the system. The calibration wheel is equipped with a Calibration Solar Diffuser (CSD) for frequent applications, a Reference Solar Diffuser (RSD) for infrequent applications, an erbium doped diffuser for spectral calibration, and a blank plate for obtaining dark current. Radiometric calibration, degradation observation, spectral calibration, and dark current acquisition using the Calibration Solar Diffuser (CSD), Reference Solar Diffuser (RSD), doped diffuser, and blank plate are then directed to the SCS optical system.

Radiometric calibration is carried out once a day, starting with dark current acquisition, CSD calibration, and ending with dark current acquisition back. CSD monitoring is carried out every month by observing CSD and RSD along one orbit. Spectral calibration is carried out every month with CSD and erbium-doped diffuser observations along one orbit. Apart from that, validation is also carried out with MODIS (Xu et al., 2020). The on-board calibration process using a solar diffuser was also carried out on the Sentinel-5 and GCOM-C satellites (Ludewig et al., 2020)(Tilstra et al., 2020)(Urabe et al., 2020). Table 3-1 lists several on-board calibrations related research.

Table 3-1. On-board calibrations related research

Camera/ Satellite	Calibration Instrument	Uncertainty	Reference
SCS/ HY-1C	Double solar diffuser and erbium-doped diffuser	< 2%	(Xu et al., 2020)
TROPOMI/ Sentinel-5 Precursor	Diffuser, white light source, spectral line source, and common LED	1 – 3%	(Ludewig et al., 2020) (Tilstra et al., 2020)
SGLI/ GCOM-C	Solar diffuser, non-polarized and polarized telescope	1%	(Urabe et al., 2020)

3.2. Rayleigh Calibration

Several radiometric calibration methods use various targets, such as deserts, ice sheets, deep convective clouds, the moon, and oceans. In the Rayleigh method, the ocean is the target. In contrast to vicarious calibration, the Rayleigh method does not require an operator to obtain the radiation. In addition, this method has the advantage that the ocean is not geographically limited and many parts of the ocean can be observed (Zhu et al., 2022).

The signal received by the sensor comes from the atmosphere and sea surface reflectance. The received reflectance is as in Equation 3-1.

$$\rho = \rho_r + \rho_a + \rho_{ra} + T\rho_{gl} + t(\rho_{sw} + \rho_{wc})\rho = \rho_r + \rho_a + \rho_{ra} + T\rho_{gl} + t(\rho_{sw} + \rho_{wc}) \quad (3\text{-}1)$$

With ρ_r representing the molecular contribution of Rayleigh distribution, ρ_a is the contribution of aerosol distribution, ρ_{ra} represents the contribution of molecular distribution between molecules and aerosols, ρ_{gl}represents the contribution of sunlight on the sea surface, T is direct transmittance, t is atmospheric diffusion transmission with ρ_{sw} and ρ_{wc} representing water leaving radiation, and white cap reflection (Zhu et al., 2019). The Rayleigh calibration procedure is shown in Figure 3-2.

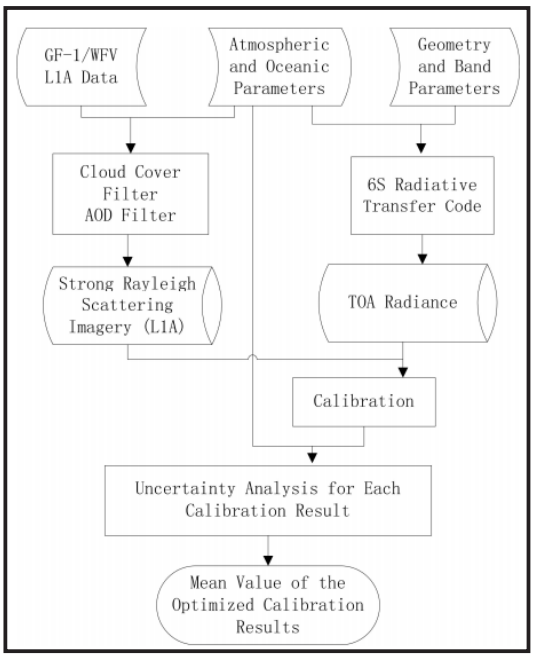

Figure 3-2. Rayleigh distribution calibration process on the Gaofen-1 satellite's Wide Field Viewing (WFV) camera (X. Chen et al., 2017)

The first step is to determine the ocean image that will be used for calibration. There are several requirements for determining image conditions, namely (a) choosing an ocean target with a small amount of chlorophyll to reduce the total reflectance of the ocean, (b) a clean atmosphere to reduce aerosol distribution, and (c) having a large solar zenith angle to increase the distribution of atmospheric molecules.

The second step is to process atmospheric and ocean parameter data for each image. The third step is to select a suitable image by considering atmospheric and oceanic parameters. The fourth step is processing images to remove clouds in the image. The fifth step is calculating the TOA radiance. The sixth step is to do analysis to optimize the calibration results (X. Chen et al., 2017). Table 3-2 lists several Rayleigh calibrations related research.

Table 3-2. Rayleigh calibrations related research

Camera/ Satellite	Calibration Site	Uncertainty	Reference
MODIS/ AQUA	Pacific Ocean	0.14 – 1.39 %	(Zhu et al., 2019)
WFV/ Gaofen-1	Southeast Pacific, Northwest Pacific, Tropical Eastern Pacific, South Indian Ocean, Tropical South Atlantic	2.44 – 4.63 %	(X. Chen et al., 2017)

3.3. Vicarious Calibration

Vicarious calibration is a calibration method in orbit using a natural target as the target instrument to be calibrated (Lin et al., 2019). In this method, atmospheric properties and

reflectance of the target surface are measured simultaneously with the satellite passing over the target. The results of these measurements are then used as input for the radiation transfer model to produce TOA radiance or TOA reflectance (Babu et al., 2023)(Tang et al., 2023) (Y.-K. Liu et al., 2020)(Jin et al., 2020)(Lin et al., 2019). The vicarious calibration method can be divided into three methods, namely the reflectance method (Babu et al., 2023)(Tang et al., 2023)(W. Chen & Wang, 2021)(Y.-K. Liu et al., 2020), radiance method (Y.-K. Liu et al., 2020), and irradiance method (Zhang et al., 2018) (W. Chen & Wang, 2021)(Tang et al., 2023).

In vicarious calibration, the data required is radiometry measurement data, atmospheric parameters, and camera images. In situ reflectance measurements were carried out using a spectroradiometer (Babu et al.,2023) (Y.-K. Liu et al., 2020), while atmospheric parameters were carried out using a sun photometer and ozonometer (Babu et al., 2023). If we use the RadCalNet calibration site, measurement data can be obtained on the AERONET website (Y.-K. Liu et al., 2020). The measurement data have almost the same time as the image data to be calibrated. The vicarious calibration process for a satellite camera is shown in Figure 3-

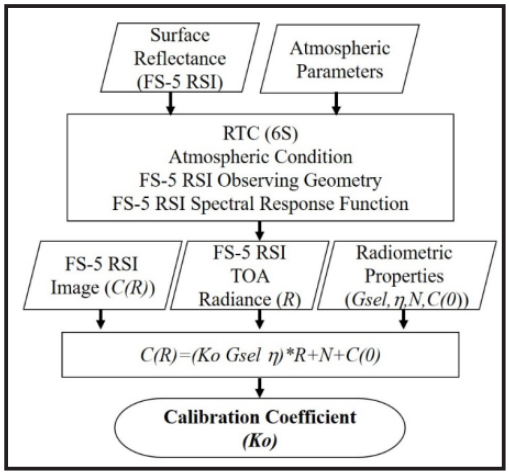

Figure 3-3. Vicarious calibration process on the Remote Sensing Instrument (RSI) payload of the Formosat-5 satellite (Lin et al., 2019)

Figure 3-3 shows a vicarious calibration method based on target reflectance measurements. The first step is to measure the surface reflectance and atmospheric parameters of the calibration site. The results of this measurement become input for the radiative transfer model to produce TOA radiance. After TOA radiance and the digital number (DN) image are known, the calibration coefficient can be obtained. The calibration coefficient is determined based on equation 3-2.

$$C(R) = (K_0 G_{sel} \eta) * R + N + C(0) C(R) = (K_0 G_{sel} \eta) * R + N + C(0) \quad (3\text{-}2)$$

C(R) is the output signal in the form of a digital number (DN); K_0 is the calibration coefficient; G_{sel} is dynamic range gain; $\eta\eta$ is the relative response of each detector; R is radiance; N is noise; and C(0) is the offset. Table 3-3 lists several vicarious calibrations related research.

Table 3-3. Vicarious calibrations related research

Camera/ Satellite	Method	Calibration Site	Uncertainty	Reference
AHSI/ Gaofen-5	Reflectance-based	Dunhuang, China	< 3%	(Tan et al., 2021)
RSI/ Formosat-5	Reflectance-based	Alkali Lake and Railroad Valley	± 5%	(Lin et al., 2019)

Camera/ Satellite	Method	Calibration Site	Uncertainty	Reference
SV0101, SV0102, SV0103, SV0104/ SuperView-1	Reflectance and radiance based	Baotou, China	4.5% for reflectance-based and 4% for radiance-based	(Y.-K. Liu et al., 2020)
MUX/ ZY3-02	Irradiance-based and reflectance based	Baotou, China	5.68% for reflectance-based and 4.06% for irradiance-based	(Tang et al., 2023)
Multispectral Imager/ Gaofen-7	Reflectance-based	Baotou, China	< 5%	(Tang et al., 2022)
AHSI/ ZY1E	Reflectance-based	Dunhuang, China	5.71%	(Yan et al., 2022)

3.4. Cross-Calibration

Cross-calibration is a method used by using sensor radiance on another satellite to identify the performance of the calibrated optical satellite sensor. This method is a general method for matching the spectral radiance of a target instrument with a reference instrument while in orbit (Wang et al., 2022). In cross-calibration, the reference camera has some requirements. The requirement is to have almost the same calibration site image, overpass time, spectral, geometry (Lu et al., 2022), and resolution (Mizuochi et al., 2020). Furthermore, the reference camera must have a stable and accurate calibration system (C. Gao et al., 2020) and easy access to images and supporting data.

In this calibration, comparisons are made between channels where the two sensors (target sensor and reference sensor) have overlapping spectral and similar response functions (Lin et al., 2019). For sensors without an on-board calibration system, cross calibration is an alternative option that is low cost, high calibration frequency, and can be carried out repeatedly to obtain calibration coefficients for each channel (H. Gao, 2016). Research on cross-calibration of satellite cameras has been widely conducted. Lu researched cross-calibration for medium resolution multispectral cameras with large angles (Lu et al., 2022). Gao researched cross-calibration to monitor VNIR sensor degradation on the Gaofen-4/GF-4 satellite using three reference sensors, namely OLI/Landsat-8, MSI/Sentinel 2, and MODIS/Terra (C. Gao et al., 2020).

Jie Han researched cross-calibration based on a radiometric block adjustment (RBA) algorithm to minimize radiometric effects due to differences in integration time (Han, Tao, Xie, Liu, et al., 2021). Mizuochi researched cross calibration with inter-band calibration on a hyperspectral camera (Mizuochi et al., 2020). The images used for cross-calibration have several criteria. Xie (Xie et al., 2017) proposed several criteria, including (a) the time difference between the target and reference images is less than 1 hour (Thome, 2001), (b) the image is not contaminated by clouds (S. Chen & Zhang, 2015), (c) the calibration site is in the center of the image (Y. Chen et al., 2017), (d) image calibration points should not be at the edges (Wolfe et al., 2002). Mizuochi proposed several criteria, including (a) the time difference between the target and reference images within 40 minutes; (b) the sensor viewing angle within 10°; (c) the angle of incidence of the sun within 6°; (d) no cloud, snow, or fog contamination. In the cross-calibration process, support data is also needed, including reflectance, water vapor, geometry, and aerosol data (Mizuochi, et.al., 2020).

Reflectance data is obtained from reference sensors, water vapor and geometry data can be obtained from MODIS products (C. Gao et al., 2020)(Mizuochi,et.al., 2020)(Han, Tao, Xie, Li, et al., 2021)(Lu et al., 2022), while aerosol data obtained from the VIIRS product (C. Gao et al., 2020). The cross-calibration method is shown in Figure 3-4.

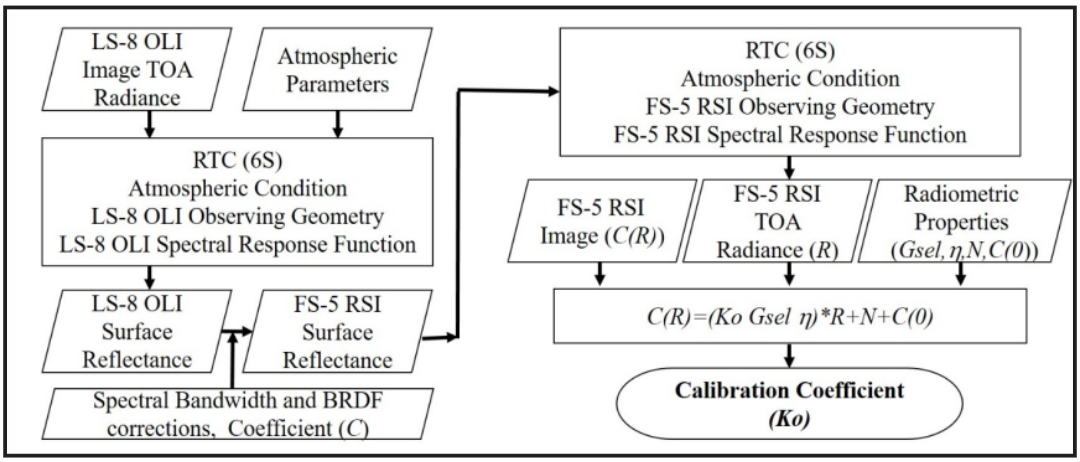

Figure 3-4. Cross-calibration of the Formosat-5 satellite's Remote Sensing Instrument (RSI) payload (Lin et al., 2019)

The first step is to select the image pair between the reference and the target sensor. The second step is to adjust the target image area to the reference image. The reference image with atmospheric parameters becomes input to the Radiative Transfer Code (RTC). The reflection of the camera surface can be determined using equation 3-3.

$$\overline{Refl_i} = \frac{\int_{\lambda_{min(i)}}^{\lambda_{max(i)}} Refl(\lambda) SRF(\lambda) d\lambda}{\int_{\lambda_{min(i)}}^{\lambda_{max(i)}} SRF(\lambda) d\lambda} \quad \ldots (3\text{-}3)$$

Where $\lambda_{max}(i)$ is the maximum wavelength of Full Width at Half Maximum (FWHM) band i, $\lambda_{min}(i)$ is the minimum wavelength of FWHM band i, Refl(λ) and SRF(λ) are surface reflectance and Spectral response at wavelength λ. The next step is to conduct spectral correction and Bidirectional Reflectance Distribution Function (BRDF) correction. The spectral difference between the reference and the target sensor can be calculated based on equation 3-4.

$$\delta_{band} = \frac{\overline{Refl_{Ref}} - \overline{Refl_{Tar}}}{Refl_{Ref}} * 100 \ldots (3\text{-}4)$$

Where $\overline{Refl_{Ref}}$ dan $\overline{Refl_{Tar}}$ are the average surface reflectance of the spectral bandwidth of the reference and the target camera. Meanwhile, the BRDF correction is calculated based on equation 3-5.

$$\delta_{viewing} = \frac{\overline{Refl_{off-nadir}} - \overline{Refl_{nadir}}}{Refl_{nadir}} * 100 \ldots (3\text{-}5)$$

Where $Refl_{off-nadir}$ dan $Refl_{nadir}$ are the surface averages at off-nadir and nadir. The spectral correction coefficient and BRDF are determined based on equation 6.

$$C = \frac{\overline{Refl_{Target\ off-nadir}}}{\overline{Refl_{Reference\ nadir}}} = (1 - \delta_{band})(1 + \delta_{viewing}) \ldots (3\text{-}6)$$

The surface reflectance from the previous process is multiplied by this coefficient to produce the surface reflectance of the target camera. This reflectance is processed with RTC to produce TOA radiance of the target camera. Next, using equation 3-2, the calibration coefficient can be found.

Apart from that, there are other methods to obtain calibration coefficients. In this method, the calibration coefficient will be calculated based on equation 3-7.

$$g_t = \frac{DN_t . \pi . d^2 . cos(\theta_R)}{SBAF . DN_R . c_R . E_t . cos(\theta_t)} \ldots (3\text{-}7)$$

Where g_t is the calibration coefficient in the form of the gain, DN_t is the digital number of the target camera, SBAF is the Spectral Band Adjustment Factor, DNR is the digital number of the reference camera, cR is the calibration gain of the reference camera, E_t is the average of solar irradiance on the target camera channel, θ_t is the sun's zenith angle on the target camera, d is the average distance between the sun and the earth, θ_R is the sun's zenith angle on the reference camera.

In this method, the SBAF is calculated based on the reflectance of the reference and target camera, which is simulated using the 6S algorithm. This process requires input in the form of ground reflectance, atmospheric parameters, and the response spectral function of the target and reference cameras to produce reflectance on the target and reference cameras. The spectral adjustment between reference and target camera is a part of cross-calibration process for avoiding systematic errors. It is producing the SBAF (C. Gao et al., 2020) (Han, Tao, Xie, Li, et al., 2021). SBAF will be calculated based on equation 3-8.

$$SBAF = \frac{\overline{Refl}_{\lambda,ref}}{\overline{Refl}_{\lambda,tar}} \quad (3\text{-}8)$$

Where $\overline{Refl}_{\lambda,ref}$ is reflectance of reference camera, and $\overline{Refl}_{\lambda,tar}$ is reflectance of target camera. Table 3-4 lists several cross-calibration related research.

Table 3-4. Cross-calibration related research

Camera/ Target Satellite	Camera/ Reference Satellite	Method	Calibration Site	Uncertainty	Reference
PMS/ Gaofen-4	OLI/ LANDSAT-8	Cross-calibration for large FOV cameras	Dunhuang (China)	1.14 – 6.65 %	(Lu et al., 2022)
VNIR/ Gaofen-4	OLI/ LANDSAT-8 MSI/ Sentinel-2 MODIS/Terra	Cross-calibration using three reference cameras	Dunhuang, Dalate, Baotou (China)	3.9 – 6.64 %	(C. Gao et al., 2020)
PMS/ Gaofen-4	OLI/ LANDSAT-8 MODIS/Terra	Cross-calibration based on radiometry block	Dunhuang (China)	0.65 – 0.97 %	(Han, Tao, Xie, Liu, et al., 2021)
EO-1/ Hyperion	MODIS/Terra	Combination of cross-calibration and inter band calibration	Railroad Valley Playa (US)	4 – 6 %	(Mizuochi et al., 2020)
PMS/ Gaofen-1	MODIS/Terra OLI/ LANDSAT-8	Cross-calibration using new model BRDF	Dunhuang and Golmud (China)	2 – 6 %	(Q. Liu et al., 2019)
WF-1/ Gaofen-1 PMS/ Gaofen-4	OLI/ LANDSAT-8	Cross-calibration using *Global Searching*	Badain Jaran (China)	0.2 – 5.6 for PMS 0,4 – 7.5 % for WF-1	(Zhou, et.al., 2021)

3.5. Comparison of Absolute Radiometric Calibration Methods

Table 3-1 shows that onboard calibration has a 1-3% uncertainty value, indicating high accuracy. This method offers the highest accuracy when compared to other approaches. The calibration instrument's performance has a significant impact on it. It will deteriorate with time, lowering the camera image's quality. Moreover, this method is limited to specific satellites equipped with an onboard calibration mechanism. Since the ocean picture target is so wide, the Rayleigh calibration works well with wide Field of View (FOV) cameras; nevertheless, this method is limited to visual channels. Table 3-2 shows that the uncertainty ranges from 0.14 to 4.63%, depending on how clean the sea target is. In addition, it is challenging in practice to pinpoint distinct images of the water.

Based on Table 3-3, the vicarious method has an uncertainty of 3–6%, depending on calibration sites and measured radiometric data. The supporting data in this method is quite accurate because the data is measured simultaneously with image acquisition by satellite. However, this method is quite expensive because it requires in-situ measurements. Especially for Indonesia, which is far from standardized calibration sites. Besides that, this method also

requires a measurement operator so there is the possibility of human error.

Meanwhile, based on Table 3-4, the cross-calibration has an uncertainty of 0.2–7.5%, depending on the calibration site and reference camera. The calibration results will be more accurate if the target and reference camera specifications are as close as possible. This method is cheap because it does not require transportation costs to the calibration site. Furthermore, it can be done frequently because it uses data from reference satellites without in-situ measurements. The weakness of this method is that it is difficult to obtain same conditions between the target and the reference camera (Kabir et al., 2020). Table 3-5 lists the strengths and weaknesses of absolute radiometric calibration methods.

Based on strengths and weaknesses, radiometric calibration methods can be adapted to satellite conditions. The onboard calibration method is suitable for satellites equipped with calibration instruments. The Rayleigh calibration method is suitable for large FOV cameras with visual wavelengths. The vicarious calibration method is suitable for satellites from countries close to standardized calibration sites. Meanwhile, the cross-calibration method is suitable for satellites cameras that have specifications and conditions close to the reference camera. Basically, these calibration methods can be carried out together to complement each method.

Table 3-5. the strengths and weaknesses of absolute radiometric calibration methods

Calibration Method	Strengths	Weaknesses
Onboard	High accuracy	Only for satellites with onboard calibration systems, the calibration instrument is degraded over time
Rayleigh	Suitable for wide Field of View (FOV) cameras	Only for visual channels, identifying specific ocean images is difficult in practice
Vicarious	Supporting data in this method is quite accurate	Expensive, requires a measurement operator so there is the possibility of human error
Cross	Cheap, coefficient calibration from this method can be updated more frequently than other methods	Difficult to obtain same conditions between the target and the reference camera

4. Conclusions

Based on the description previously, onboard calibration is a relatively accurate method with a range value that is not significant, with an uncertainty value of 1-3%. However, in some conditions, Rayleigh and cross-calibration are more accurate than onboard calibration because these methods have low uncertainty values, namely 0.14% and 0.2%, depending on calibration sites (Rayleigh and cross), as well as reference camera (cross). Basically, all methods can be used and adapted to the conditions of the satellite. The onboard calibration method is suitable for satellites equipped with calibration instruments. The Rayleigh calibration method is suitable for large FOV cameras with visual wavelengths. The vicarious calibration method is suitable for satellites from countries close to standardized calibration sites. Meanwhile, the cross-calibration method is suitable for satellites cameras that have specifications and conditions close to the reference camera. Therefore, these calibration methods can be carried out together to complement each method.

Acknowledgements

The author would like to thank Mr. Mohammad Mukhayadi and Mr. Patria Rachman Hakim as group leader and leader satellite operation missions of Satellite Technology Research Center BRIN, for their support and assistance so that this works can be well completed.

Contributorship Statement

Sartika Salaswati, Adhi Harmoko Saputro, and Wahyudi Hasbi have the same role as the main contributors in this research, who are responsible for the research design process and analysis of literature review.

References

Agency, E. S. (2015). *Sentinel-2 User Handbook*. ESA Standard Document.

Amalo, L. F., Nur, I. A., & Rochimawati, N. R. (2019). Drought monitoring using LISAT (LAPAN-IPB Satellite) and Landsat 8 Satellite Imagery in Pakisjaya District, West Java. *IOP Conference Series: Earth and Environmental Science*, *284*(1). https://doi.org/10.1088/1755-1315/284/1/012008

Arai, K. (2013). Comparison Among Cross, Onboard and Vicarious Calibrations for Terra/ASTER/VNIR. *International Journal of Advanced Research in Artificial Intelligence*, *2*(10), 14–18. https://doi.org/10.14569/ijarai.2013.021003

Ariza Ramirez, W., Mishra, G., Panda, B. K., Jung, H. W., Lee, S. H., Lee, I., & Singh, C. B. (2022). Multispectral camera system design for replacement of hyperspectral cameras for detection of aflatoxin B1. *Computers and Electronics in Agriculture*, *198*(May), 107078. https://doi.org/10.1016/j.compag.2022.107078

Babu, K. N., Kumawat, N., & Pandya, M. R. (2023). Radiometric Calibration of AVIRIS-NG sensor using Indian desert sites. *Advances in Space Research*, *xxxx*. https://doi.org/10.1016/j.asr.2023.01.022

Bolívar-Santamaría, S., & Reu, B. (2021). Detection and characterization of agroforestry systems in the Colombian Andes using sentinel-2 imagery. *Agroforestry Systems*, *95*(3), 499–514. https://doi.org/10.1007/s10457-021-00597-8

Chen, S., & Zhang, T. (2015). An improved cloud masking algorithm for MODIS ocean colour data processing. *Remote Sensing Letters*, *6*(3), 218–227. https://doi.org/10.1080/2150704X.2015.1026955

Chen, W., & Wang, H. (2021). Absolute radiometric calibration and validation of a UAV multispectral sensor: a comparison between the irradiance-based method and reflectance-based method. *Journal of Spatial Science*, *66*(3), 481–492. https://doi.org/10.1080/14498596.2019.1658651

Chen, X., Xing, J., Liu, L., Li, Z., Mei, X., Fu, Q., Xie, Y., Ge, B., Li, K., & Xu, H. (2017). In-flight calibration of GF-1/WFV visible channels using Rayleigh scattering. *Remote Sensing*, *9*(6). https://doi.org/10.3390/rs9060513

Chen, Y., Sun, K., Li, D., Bai, T., & Huang, C. (2017). Radiometric cross-calibration of GF-4 PMS sensor based on assimilation of landsat-8 OLI images. *Remote Sensing*, *9*(8), 1–19. https://doi.org/10.3390/rs9080811

Fadaei, H. (2020). Advanced land observing satellite data to identify ground vegetation in a juniper forest, northeast Iran. *Journal of Forestry Research*, *31*(2), 531–539. https://doi.org/10.1007/s11676-018-0812-5

Gao, C., Liu, Y., Qiu, S., Li, C., Ma, L., Han, Q., Liu, J., & Zhao, E. (2020). *Radiometric Cross-Calibration of GF-4 / VNIR Sensor*. *13*, 2337–2350.

Gao, H. (2016). *Cross-Calibration of GF-1 PMS Sensor With*. *54*(8), 4847–4854.

Hakim, P. R., Syafrudin, A. H., Salaswati, S., Utama, S., & Hasbi, W. (2019). *Development of Systematic Image Preprocessing of LAPAN-A3/IPB Multispectral Images*. *7*(10), 9–18. http://arxiv.org/abs/1901.09189

Han, J., Tao, Z., Xie, Y., Li, H., Liu, Q., & Guan, X. (2021). A Novel Radiometric Cross-Calibration of GF-6/WFV with MODIS at the Dunhuang Radiometric Calibration Site. *IEEE Journal of Selected Topics in Applied Earth Observations and Remote Sensing*, *14*, 1645–1653. https://doi.org/10.1109/JSTARS.2020.3046738

Han, J., Tao, Z., Xie, Y., Liu, Q., & Huang, Y. (2021). Radiometric Cross-Calibration of GF-4/PMS Based on Radiometric Block Adjustment. *IEEE Transactions on Geoscience and Remote Sensing*, *59*(6), 4522–4534. https://doi.org/10.1109/TGRS.2020.3009740

Hao, Q., Song, Y., Cao, J., Liu, H., Liu, Q., Li, J., Luo, Q., Cheng, Y., Cui, H., & Liu, L. (2023). The Development of Snapshot Multispectral Imaging Technology Based on Artificial Compound Eyes. *Electronics (Switzerland)*, *12*(4). https://doi.org/10.3390/electronics12040812

Jin, C., Ahn, H., Seo, D., & Choi, C. (2020). *Radiometric Calibration and Uncertainty Analysis of KOMPSAT-3A Using the Reflectance-Based Method*.

Justice, C. O., Townshend, J. R. G., Vermote, E. F., Masuoka, E., Wolfe, R. E., Saleous, N., Roy, D. P., & Morisette, J. T. (2002). An overview of MODIS Land data processing and product status. *Remote Sensing of Environment*, *83*(1–2), 3–15. https://doi.org/10.1016/S0034-4257(02)00084-6

Kabir, S., Leigh, L., & Helder, D. (2020). Vicarious methodologies to assess and improve the quality of the optical remote sensing images: A critical review. *Remote Sensing*, *12*(24), 1–40. https://doi.org/10.3390/rs12244029

Lin, T. H., Chang, J. C., Hsu, K. H., Lee, Y. S., Zeng, S. K., Liu, G. R., Tsai, F. A., & Chan, H. P. (2019). Radiometric variations of On-Orbit FORMOSAT-5 RSI from vicarious and cross-calibration measurements. *Remote Sensing*, *11*(22). https://doi.org/10.3390/rs11222634

Liu, C. C., Chen, Y. H., Wu, M. H. M., Wei, C., & Ko, M. H. (2019). Assessment of forest restoration with multitemporal remote sensing imagery. *Scientific Reports*, *9*(1), 1–19. https://doi.org/10.1038/s41598-019-43544-5

Liu, Q., Yu, T., & Gao, H. (2019). Radiometric cross-calibration of gf-1 pms sensor with a new brdf model. *Remote Sensing*, *11*(6), 1–22. https://doi.org/10.3390/RS11060707

Liu, Y.-K., Ma, L.-L., Wang, N., Qian, Y.-G., Zhao, Y.-G., Qiu, S., Gao, C.-X., Long, X.-X., & Li, C.-R. (2020). On-orbit radiometric calibration of the optical sensors on-board SuperView-1 satellite using three independent methods. *Optics Express*, *28*(8), 11085. https://doi.org/10.1364/oe.388387

Liu, Y., Ma, Z., Ma, L., Wang, N., Qian, Y., & Li, C. (2018). *VICARIOUS RADIOMETRIC CALIBRATION USING A GROUND RADIANCE-BASED APPROACH : A CASE STUDY OF SENTINEL 2A MSI Key Laboratory of Quantitative Remote Sensing Information Technology , Academy of Opto-Electronics , Corresponding author : kevin_rser@163.cn*. 3296–3299.

Lu, J., He, T., Liang, S., & Zhang, Y. (2022). An Automatic Radiometric Cross-Calibration Method for Wide-Angle Medium-Resolution Multispectral Satellite Sensor Using Landsat Data. *IEEE Transactions on Geoscience and Remote Sensing*, *60*, 1–11. https://doi.org/10.1109/TGRS.2021.3067672

Ludewig, A., Kleipool, Q., Bartstra, R., Landzaat, R., Leloux, J., Loots, E., Meijering, P., Van Der Plas, E., Rozemeijer, N., Vonk, F., & Veefkind, P. (2020). In-flight calibration results of the TROPOMI payload on board the Sentinel-5 Precursor satellite. *Atmospheric Measurement Techniques*, *13*(7), 3561–3580. https://doi.org/10.5194/amt-13-3561-2020

Mishra, G., Panda, B. K., Ramirez, W. A., Jung, H., Singh, C. B., Lee, S. H., & Lee, I. (2022). Application of SWIR hyperspectral imaging coupled with chemometrics for rapid and non-destructive prediction of Aflatoxin B1 in single kernel almonds. *Lwt*, *155*(August 2021), 112954. https://doi.org/10.1016/j.lwt.2021.112954

Mizuochi, H., Tsuchida, S., Obata, K., Yamamoto, H., & Yamamoto, S. (2020). Combination

of cross-and inter-band radiometric calibrations for a hyperspectral sensor using model-based spectral band adjustment. *Remote Sensing*, *12*(12). https://doi.org/10.3390/rs12122011

Parveen, M. T., & Ilahi, R. A. (2022). Assessment of land-use change and its impact on the environment using GIS techniques: a case of Kolkata Municipal Corporation, West Bengal, India. *GeoJournal*, *87*(s4), 551–566. https://doi.org/10.1007/s10708-022-10581-z

Permatasari, P. A., Muslimah, S., & Utomo, B. A. (2019). Comparison of LISAT and Landsat imagery for estimating chlorophyll-a (case study: Jatiluhur Reservoir). *IOP Conference Series: Earth and Environmental Science*, *284*(1). https://doi.org/10.1088/1755-1315/284/1/012041

Prasad, A. D., Ganasala, P., Hernández-Guzmán, R., & Fathian, F. (2022). Remote sensing satellite data and spectral indices: an initial evaluation for the sustainable development of an urban area. *Sustainable Water Resources Management*, *8*(1), 1–16. https://doi.org/10.1007/s40899-022-00607-2

Raimadoya, M. A., Trisasongko, B. H., & Zain, A. (2011). Analisis Misi Dan Rancangan Lapan-Ipb Satellite (Lisat) Untuk Pemantauan Kemandirian Pangan. *Jurnal Ilmu Pertanian Indonesia*, *16*(3), 173–178.

Ridwan, M. A., Radzi, N. A. M., Ahmad, W. S. H. M. W., Mustafa, I. S., Din, N. M., Jalil, Y. E., Isa, A. M., Othman, N. S., & Zaki, W. M. D. W. (2018). Applications of landsat-8 data: A Survey. *International Journal of Engineering and Technology(UAE)*, *7*(4), 436–441. https://doi.org/10.14419/ijet.v7i4.35.22858

Ryan, R., & Pagnutti, M. (2009). Enhanced absolute and relative radiometric calibration for digital aerial cameras. *Photogrammetric Week*, 81–90. http://scholar.google.com/scholar?hl=en&btnG=Search&q=intitle:Enhanced+Absolute+and+Relative+Radiometric+-Calibration+for+Digital+Aerial+Cameras#0

Setiawan, Y., Prasetyo, L. B., Pawitan, H., Liyantono, L., Syartinilia, S., Wijayanto, A. K., Permatasari, P. A., Syafrudin, A. H., & Hakim, P. R. (2018). Pemanfaatan Fusi Data Satelit Lapan-a3/Ipb Dan Landsat 8 Untuk Monitoring Lahan Sawah. *Jurnal Pengelolaan Sumberdaya Alam Dan Lingkungan (Journal of Natural Resources and Environmental Management)*, *8*(1), 67–76. https://doi.org/10.29244/jpsl.8.1.67-76

Sharifi, A., Felegari, S., & Tariq, A. (2022). Mangrove forests mapping using Sentinel-1 and Sentinel-2 satellite images. *Arabian Journal of Geosciences*, *15*(20). https://doi.org/10.1007/s12517-022-10867-z

Tamang, M., Nandy, S., Srinet, R., Das, A. K., & Padalia, H. (2022). Bamboo Mapping Using Earth Observation Data: A Systematic Review. *Journal of the Indian Society of Remote Sensing*, *50*(11), 2055–2072. https://doi.org/10.1007/s12524-022-01600-0

Tan, K., Wang, X., Niu, C., Wang, F., Du, P., Sun, D. X., Yuan, J., & Zhang, J. (2021). Vicarious Calibration for the AHSI Instrument of Gaofen-5 with Reference to the CRCS Dunhuang Test Site. *IEEE Transactions on Geoscience and Remote Sensing*, *59*(4), 3409–3419. https://doi.org/10.1109/TGRS.2020.3014656

Tang, H., Xie, J., Chen, W., Zhang, H., & Wang, H. (2023). *Absolute Radiometric Calibration of ZY3-02 Satellite Multispectral Imager Based on Irradiance-Based Method*.

Tang, H., Xie, J., Tang, X., Chen, W., & Li, Q. (2022). On-Orbit Radiometric Performance of GF-7 Satellite Multispectral Imagery. *Remote Sensing*, *14*(4), 1–18. https://doi.org/10.3390/rs14040886

Thakur, S., Mondal, I., Ghosh, P. B., Das, P., & De, T. K. (2020). A review of the application of multispectral remote sensing in the study of mangrove ecosystems with special emphasis on image processing techniques. *Spatial Information Research*, *28*(1), 39–51. https://doi.org/10.1007/s41324-019-00268-y

Thome, K. J. (2001). Absolute radiometric calibration of Landsat 7 ETM+ using the reflectance based method. *Remote Sensing of Environment*, *78*, 27–38.

Tilstra, L. G., Graaf, M. De, Wang, P., & Stammes, P. (2020). In-orbit Earth reflectance validation

of TROPOMI on board the Sentinel-5 Precursor satellite. *Atmospheric Measurement Techniques*, *13*(8), 4479–4497. https://doi.org/10.5194/amt-13-4479-2020

Urabe, T., Xiong, X., Hashiguchi, T., Ando, S., Okamura, Y., & Tanaka, K. (2020). Radiometric model and inter-comparison results of the SGLI-VNR on-board calibration. *Remote Sensing*, *12*(1). https://doi.org/10.3390/rs12010069

Wang, Q., Zhang, P., Member, S., Xu, N., Chen, L., Wu, R., Liu, J., & Si, F. (2022). *An Investigation on Inter-Calibrating EMI / GF-5 With TROPOMI / S5p in Ultraviolet – Visible Spectra*. *60*.

Wijayanto, A. K., Yusuf, S. M., & Pambudi, W. A. (2019). The Characteristic of spectral reflectance of LAPAN-IPB (LAPAN-A3) Satellite and Landsat 8 over agricultural area in Probolinggo, East Java. *IOP Conference Series: Earth and Environmental Science*, *284*(1). https://doi.org/10.1088/1755-1315/284/1/012004

Wolfe, R. E., Nishihama, M., Fleig, A. J., Kuyper, J. A., Roy, D. P., Storey, J. C., & Patt, F. S. (2002). Achieving sub-pixel geolocation accuracy in support of MODIS land science. *Remote Sensing of Environment*, *83*(1–2), 31–49. https://doi.org/10.1016/S0034-4257(02)00085-8

Xie, Y., Han, J., Gu, X., & Liu, Q. (2017). On-orbit radiometric calibration for a space-borne multi-camera Mosaic imaging sensor. *Remote Sensing*, *9*(12), 1–19. https://doi.org/10.3390/rs9121248

Xu, H., Zhang, L., Huang, W., Li, X., Si, X., Xu, W., & Song, Q. (2020). On-Board Absolute Radiometric Calibration and Validation Based on Solar Diffuser of HY-1C SCS. *Guangxue Xuebao/Acta Optica Sinica*, *40*(9), 30015–30034. https://doi.org/10.3788/AOS202040.0928002

Yan, L., Li, J., & Xiao, C. (2022). Vicarious Radiometric Calibration of the AHSI Instrument Onboard ZY1E on Dunhuang Radiometric Calibration Site. *IEEE Transactions on Geoscience and Remote Sensing*, *60*. https://doi.org/10.1109/TGRS.2022.3180120

Zhang, H., Zhang, B., Chen, Z., & Huang, Z. (2018). Vicarious radiometric calibration of the hyperspectral imaging microsatellites SPARK-01 and -02 over Dunhuang, China. In *Remote Sensing* (Vol. 10, Issue 1). https://doi.org/10.3390/rs10010120

Zhu, S., Chen, X., Liu, L., Qie, L., Li, Z., Ma, J., Ge, S., Hong, J., Li, X., & Gao, H. (2019). Evaluation of radiometric performance of MODIS visible bands using the Rayleigh scattering method. *Journal of Applied Remote Sensing*, *13*(01), 1. https://doi.org/10.1117/1.jrs.13.018503

Zhu, S., Li, Z., Qie, L., Xu, H., Ge, B., Xie, Y., Qiao, R., Xie, Y., Hong, J., Meng, B., Tu, B., & Chen, F. (2022). In-Flight Relative Radiometric Calibration of a Wide Field of View Directional Polarimetric Camera Based on the Rayleigh Scattering over Ocean. *Remote Sensing*, *14*(5), 1–19. https://doi.org/10.3390/rs14051211

.